Check for updates

A skyrmionic topology perspective on Lehmann clusters

Pawel Pieranski, (ID) *[a] Ivan Smalyukh, (ID) [bc] Mehdi Zeghal,[a] Patrick Judeinstein (ID) [d] and Maria Helena Godinho (ID) [e]

When two parallel coplanar dislocations with opposite Burgers vectors are brought into collision by the action of stress in solid crystals, they annihilate each other. In cholesterics with pitch p, under certain conditions, colliding dislocations with Burgers vectors $b = p$ and $b = -p$ are immune against annihilation and form stable twin-like pairs known as Lehmann clusters. We point out that this immunity is due to the escape of the director field into the third dimension. We show that from a topological point of view, Lehmann clusters can be seen as skyrmion tubes embedded in a helicoidal background, and their extremities have the topology of monopoles.

1 Collisions of parallel coplanar dislocation

1.1 Annihilation of dislocation pairs in solid crystals

In solid crystals, two parallel coplanar dislocations with opposite Burgers vectors, when driven into collision by stress, annihilate each other, as shown schematically in Fig. 1.

1.2 Lehmann clusters: twin-like pairs of cholesteric dislocations immune against annihilation

Experiments by Smalyukh and Lavrentovich (S & L) with cholesterics confined between surfaces with planar anchorings[1] have shown that under certain conditions, two parallel coplanar dislocations can be immune against annihilation and form stable twin-like pairs. Using confocal polarizing fluorescence microscopy, S & L have found that such stable pairs are composed of dislocations with opposite Burgers vectors $b = p$ and $b = -p$, where p is the cholesteric pitch (see Fig. 2–4 and 6).

Inspired by the pioneering work of Kleman and Friedel,[2] S & L proposed models for the director field of stable pairs. As shown in Fig. 3, they consist of sets of four disclinations $\{\lambda^{+1/2}, \lambda^{-1/2}, \lambda^{-1/2}, \text{ and } \lambda^{+1/2}\}$ or $\{\tau^{+1/2}, \tau^{-1/2}, \tau^{-1/2}, \text{ and } \tau^{+1/2}\}$ located at vertices of a rhombus. Knowing that such clusters of four disclinations were observed already by Otto Lehmann,[3,4]

[a] Laboratoire de Physique des Solides, Université Paris-Saclay, 91405 Orsay, France.
  E-mail: pawel.pieranski@universite-paris-saclay.fr
[b] Department of Physics, University of Colorado, Boulder, CO 80309-0390, USA
[c] International Institute for Sustainability with Knotted Chiral Meta Matter
  (WPI-SKCM2), 2-313 Kagamiyama, Higashi-Hiroshima City, Hiroshima, Japan
[d] Université Paris-Saclay, CEA, CNRS, LLB, 91191 Gif-sur-Yvette, France
[e] i3N/CENIMAT, Department of Materials Science, NOVA School of Science and
  Technology, NOVA University Lisbon, Campus de Caparica, Caparica 2829-516,
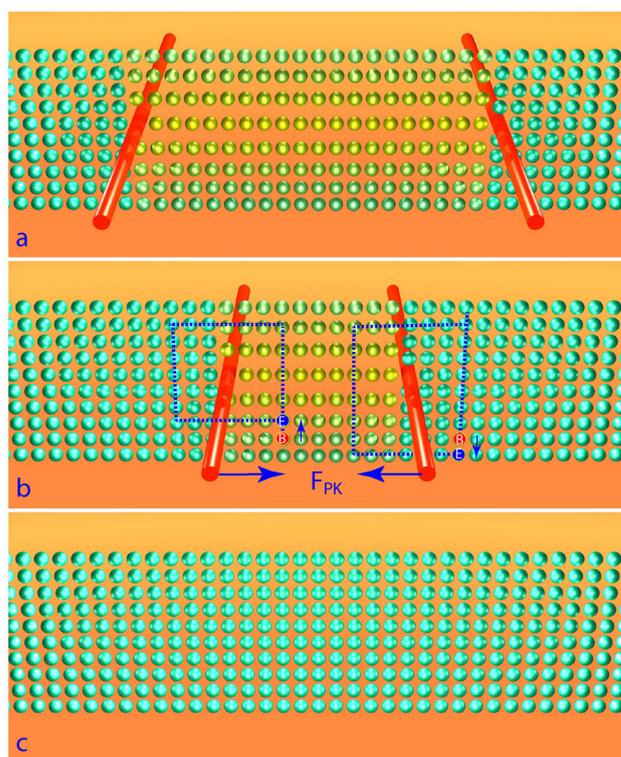 *Portugal*

Fig. 1 Annihilation of a pair of parallel coplanar edge dislocations with opposite Burgers vectors in a solid crystal. (a) Initial position of dislocations. (b) Due to the action of Peach–Koehler forces, the distance between dislocations decreases. (c) After collision of dislocations resulting in their annihilation, the crystal is defect-free.

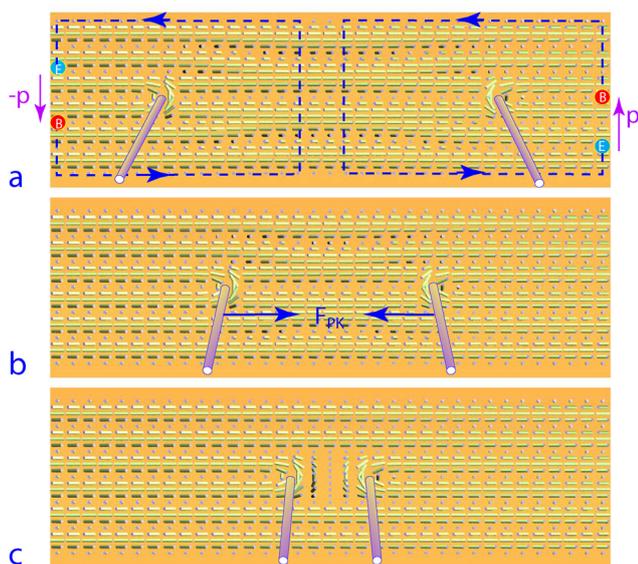S & L proposed to call the stable pairs of dislocation "Lehmann clusters".

Fig. 2 Generation of a Lehman cluster. (a) Pair of dislocations with opposite Burgers vectors $b = p$ and $b - p$ in a cholesteric layer. (b) Due to the action of Peach–Koehler forces, the distance between dislocations decreases. (c) Upon collision, the dislocations do not annihilate but form a stable twin-like pair known as Lehmann cluster.
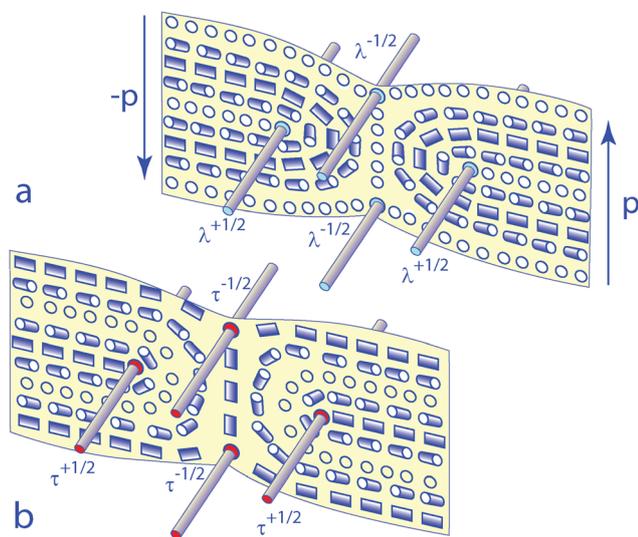

Fig. 3 Models of the director field of the Lehmann cluster proposed by Smalyukh and Lavrentovich:[1] (a) four non-singular disclinations λ and (b) four singular disclinations τ.

1.3 Role of the Lehmann clusters in the stability of tangles, knots and links

Since the generic work of Smalyukh and Lavrentovich,[1] twin-like pairs of dislocations immune against annihilation were also observed in experiments with tangles,[5] knots[6] and links[7,8] made of cholesteric dislocations with the Burgers vector b equal to the full (2π) pitch p. Crossings in such knots and links frequently have the structure of Lehmann clusters. Therefore, the immunity of tangles, knots and links against
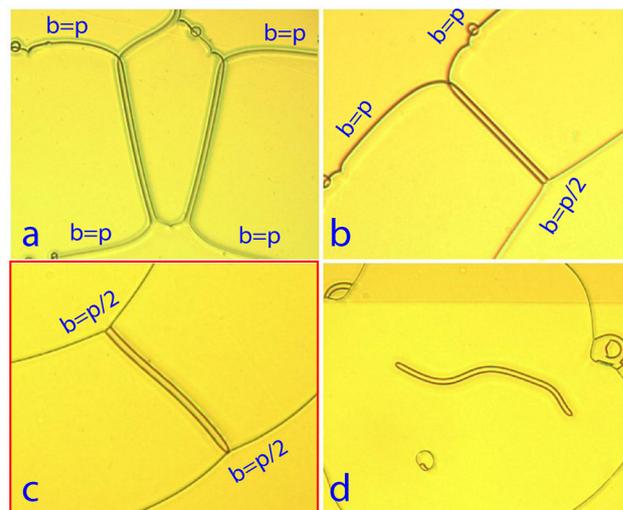

Fig. 4 Occurrence of Lehmann clusters. (a) As crossings of $b = p$ dislocations. (b) Spanned between the $b = p$ and $b = p/2$ dislocations. (c) Spanned between two $b = p/2$ dislocations. This type of Lehmann cluster is considered in detail in this paper. (d) As a closed worm-like loop equivalent to a skyrmion tube (see Section 6.2).

the rewiring is similar to that of the Lehmann clusters discussed here.

1.4 Occurrence of Lehmann clusters

The occurrence of Lehmann clusters in patterns of dislocations in cholesterics confined in gaps of variable thickness is summarized in Fig. 4 and can be classified into four types (see also the S & L article[1]):

Type 1: they can appear as crossings between $b = p$ dislocations (see Fig. 4a).

Type 2: they can be spanned between $b = p$ and $b = p/2$ dislocations (see Fig. 4b).

Type 3: they can be spanned between two $b = p/2$ dislocations (see Fig. 4c). This paper is devoted to this type of Lehmann cluster.

Type 4: they can be independent. In this case, they form worm-like narrow loops (see Fig. 4d) and are not stable because the length of such loops decreases in time until the final collapse occurs.

1.5 Aims of this paper

In the present paper, we will explain the immunity of the Lehmann clusters against annihilation (or rewiring) in terms of an alternative, singularity-free solitonic model of the director field resulting from the escape into the third dimension.

Before these theoretical considerations in Section 3, we will report in the next Section 2 on new experiments focussed on a controlled generation of Lehmann clusters of type 4.

2 Experimental

2.1 Haphazard occurrence of Lehmann clusters

It is well known that cholesterics confined in gaps of variable thickness contain dislocation patterns made of $b = p/2$ and

$b = p$ dislocations. In the sphere/plane geometry, the ground state consists of separated concentric circular dislocation loops. In practice, this ideal ground state configuration is rather rare because after preparation involving flows and/or isotropic → cholesteric transition, the cholesteric droplets contain dense skeins of knotted and linked dislocations that decay slowly by rewiring of crossings. On long time scale, the decay process leads to metastable patterns of interconnected loops.

Most frequently, the circular loops are interconnected by crossings such as those in Fig. 4a so that the dislocation patterns can contain knots or links. Connections of the $b = p/2$ dislocation loops by Lehmann clusters (Fig. 4c) can exist as well, but beside the generic work of S & L,[1] little attention has been paid to them.

Obviously, the production of Lehmann clusters by the decay of random skeins of dislocations is haphazard. The setup described below was tailored for a more efficient production of Lehmann clusters.

2.2 Setup

The setup represented in Fig. 5a is a modified version of the one used previously in experiments with tangles,[5] knots[6,9] and links.[7]

It consists of two mica sheets, supported and bent into cylindrical shapes by plastic parts described in detail previously.[6,8] The small vertical distance h_{min} between the mica sheets is controlled with an accuracy of 0.5 μm by means of a micrometric translation stage.[6,8] The cholesteric sample – a droplet of the 5CB/CB15 mixure (see Section 3 of the SI) – is confined by capillarity inside the gap between the mica sheets.

With the aim to melt the cholesteric sample into the isotropic phase, the setup was modified by the addition of a system blowing a jet of hot nitrogen gas ($T \approx 40$ °C) on the upper mica sheet through a conical nozzle (a micro-pipette tip) as shown in Fig. 5a.

After the melting of the sample into the isotropic phase, the hot nitrogen jet is switched off and the cholesteric phase is recovered by spontaneous cooling at ambient temperature ($T \approx 20$ °C). Due to the very small thicknesses of the mica sheets and of the cholesteric droplet (≈ 100 μm), the characteristic times of heating and cooling are of the order of magnitude ≈ 1 s. The size of the area heated by the hot gas depends on the vertical distance between the pipette tip and the upper mica sheet. Typically, its diameter is of the order of 2 mm.

2.3 Generation of Lehmann clusters

In the experiment represented in Fig. 5b–d, the cholesteric droplet contains initially (see Fig. 5b) three circular concentric $b = p/2$ dislocation loops interconnected already by seven Lehmann clusters. The $b = p/2$ loops separate fields labeled with indices N corresponding to the number of full cholesteric pitches located between the mica sheets.

This initial pattern is heated locally and briefly by a hot nitrogen jet. The size of the area in which the cholesteric → isotropic melting occurred is on the order of 2 mm. After cooling back into the cholesteric phase, this area contains dense skeins of dislocations (see Fig. 5c). The elastic relaxation of these skeins lasts about 550 s and leads to formation of a new Lehmann cluster visible in Fig. 5d. Remark: generation of a Lehmann cluster by just one sequence of cholesteric → isotropic → cholesteric phase transitions is not guaranteed. In practice, the experiment must be repeated several times until the new Lehmann cluster is created.
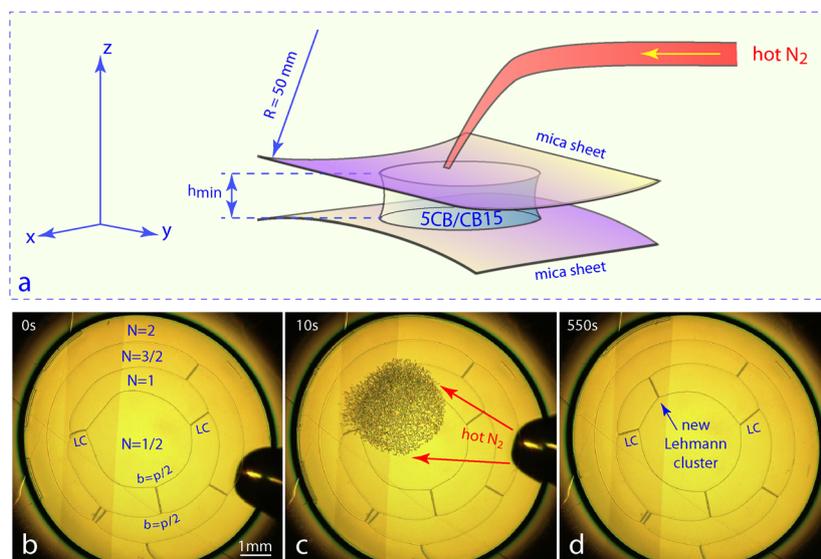

Fig. 5 Controlled generation of Lehmann clusters. (a) Experimental setup. (b) Eight Lehmann clusters spanned between circular $b = p/2$ dislocation loops. N is the number of full cholesteric pitches located between the mica sheets. (c) Dense skein of dislocations generated locally by the sequence of phase transitions: cholesteric → isotropic → cholesteric. (d) After relaxation, a new Lehmann cluster appears. Like the initial eight ones, it is spanned between two $b = p/2$ loops (see Videos S1 and S2 of the SI).

2.4 Structure of Lehmann clusters

In the simplest case, the Lehmann cluster has the structure depicted in Fig. 6. It is spanned inside the annular field labeled as N between two circular $b = p/2$ dislocations. One of them is visible in Fig. 6a and b. The second one, separating fields with $N = 1$ and $N = 3/2$ pitches, is located outside of the area visible in Fig. 6a.

This Lehmann cluster itself is made of a pair of $b = p$ and $b = -p$ parallel dislocations separating fields with $N = 1$ and $N = 0$ cholesteric pitches (see Fig. 6b). The two dislocations are pushed one against the other by Peach–Koehler forces F_{PK} determined by the local thickness as discussed below. The equilibrium distance δ between them is determined by the balance between this Peach–Koehler force F_{PK} and the force F_{el} of the repulsive elastic interaction which grows with the inverse of the distance δ between the dislocations.

Independently of quantitative details concerning the equilibrium distance δ, we will point out in Section 3 that δ cannot tend to zero because the pair of dislocation of this Lehmann cluster is protected topologically against annihilation.

2.5 Splitting of the Lehmann cluster

Let us consider the experiment represented in Fig. 7 where a Lehmann cluster is spanned inside the central $b = p/2$ loop. This experiment shows that the Lehmann cluster is stable as long as the minimal thickness h_{min} between the cylindrical
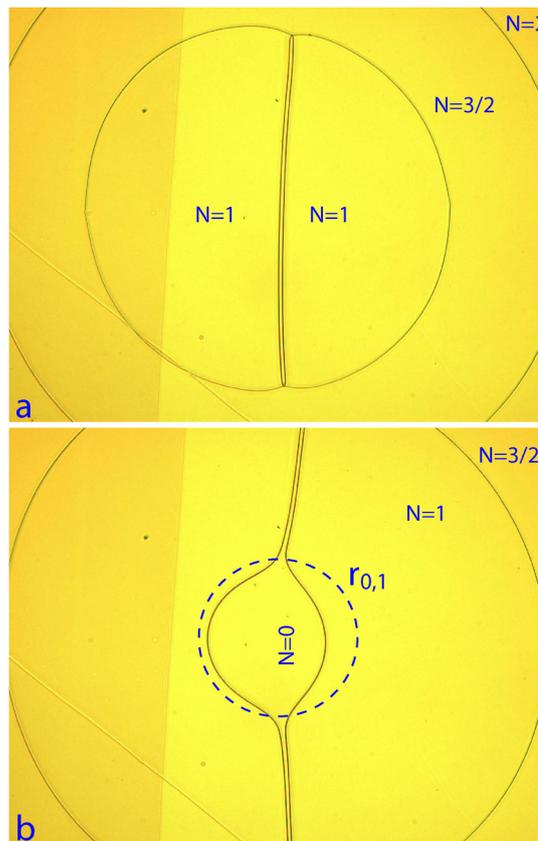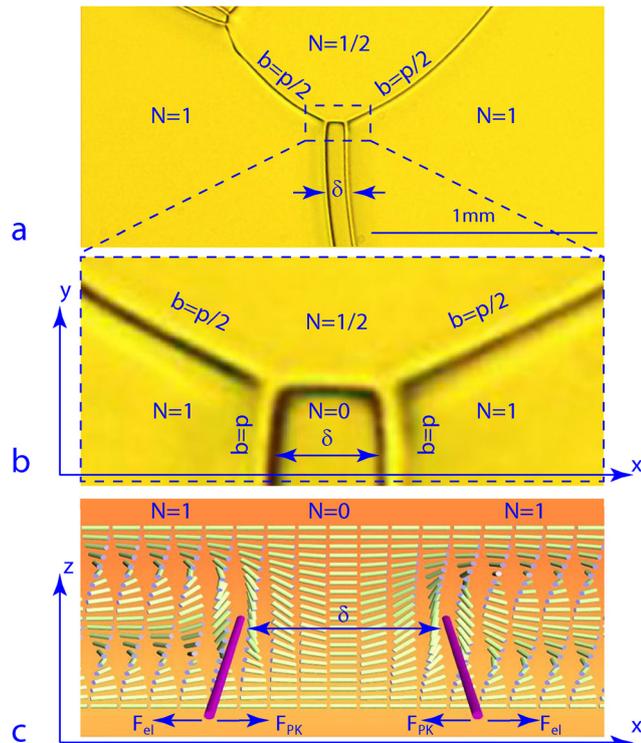

Fig. 6 Structure of Lehmann clusters. (a) Junction between a Lehmann cluster and a $p/2$ dislocation loop. (b) Close-up of the junction. (c) Defect-free variant of the director field in the (x,z) cross-section of the Lehmann cluster (see Section 3).

Fig. 7 Splitting of the Lehmann cluster upon reduction of the thickness h_{min}. (a) $h_{min} > p_o/2$. (b) $h_{min} < p_o/2$ (see Video 4 of the SI).

mica sheets is larger than $p_o/2$ where p_o is the equilibrium cholesteric pitch which is the case in Fig. 7a. By the way, let us note that the stability of the central dislocation loop depends also on the minimal thickness h_{min}; for $h_{min} > 3p_o/4$, it collapses.

Upon reduction of the minimal thickness h_{min} below $p_o/2$, the twin dislocations of this Lehmann cluster separate one from the other and tend to adopt the circular shape of radius $r_{0,1}$ as shown in Fig. 7b.

2.6 Peach–Koehler force

This behavior is determined by the dependence of the Peach–Koehler force on the local thickness h. This force per unit length corresponds to the difference between the densities of the distortion energy per unit area on the two sides of the twin dislocations. On the side with $N = 0$, one has

$$f_0 = h\frac{K_{22}}{2}\left(\frac{2\pi}{p_o}\right)^2 \tag{1}$$

(K_{22} is the twist elastic coefficient), while on the other side with $N = 1$, one has

$$f_1 = h\frac{K_{22}}{2}\left(\frac{2\pi}{h} - \frac{2\pi}{p_o}\right)^2 = h\frac{K_{22}}{2}\left(\frac{2\pi}{p_o}\right)^2\left(\frac{p_o}{h} - 1\right)^2 \tag{2}$$

The Peach–Koehler is thus

$$F_{PK} = f_1 - f_0 = p_o \frac{K_{22}}{2} \left(\frac{2\pi}{p_o}\right)^2 \left(\frac{p_o}{h} - 2\right) \qquad (3)$$

It changes sign for $h = p_o/2$.

In the cylinder/cylinder geometry, where the thickness h varies with the distance r from the gap center as

$$h(r) \approx h_{min} + \frac{r^2}{2R} \qquad (4)$$

the sign of the Peach–Koehler force changes on the circle of radius

$$r_{0,1} \approx \sqrt{2R(p_o/2 - h_{min})} \qquad (5)$$

which is drawn with a dashed line shown in Fig. 7b.

For $r > r_{0,1}$, the Peach–Koehler force pushes the twin dislocations one against the other and the Lehmann cluster is stable.

For $r < r_{0,1}$, the Lehman cluster splits and the two twin dislocations tend to take semi-circular shapes of radius $r_{0,1}$ for which the Peach–Koehler force vanishes.

Deviations from these ideal linear and circular shapes are due to the Laplace force given by

$$F_{Lap} = \frac{T_{0,1}}{\rho} \qquad (6)$$

where $T_{0,1}$ is the tension of dislocations and ρ is the radius of their local curvature. Their discussion is out of the scope of this paper.

3 Topological immunity of Lehmann clusters against annihilation

As we will see below, the topological immunity against annihilation of the dislocation pairs forming Lehmann clusters is related to the singularity-free director fields of the individual dislocations themselves. Such singularity-free fields can be constructed by the geometrical method illustrated in Fig. 8 and discussed in detail in Section 1.1 of the SI, where it is applied to the simplest case of a $b = p$ dislocation separating fields with $N = 1$ and $N = 0$ cholesteric pitches as discussed above (see Fig. 6).

3.1 B variant of the singularity-free director field of dislocations with the Burgers vector $b = p$

Let us consider first the field $\mathbf{n}_B(x,z)$ in Fig. 8a labeled as "B". It can be seen as a wall of width λ across which the cholesteric helix $\mathbf{n}(0, z) = (\cos(2\pi z/p), \sin(2\pi z/p), 0)$, depicted in column 1, is deformed continuously into the homogeneous field $\mathbf{n}(\lambda,z) = (1,0,0)$ depicted in column 8.

When the field $\mathbf{n}_B(x,z)$ is mapped onto the unit sphere in Fig. 8b, the whole north hemisphere is covered. In particular, column 1 with $\mathbf{n}_B(0,z) = (\cos(2\pi z/p),\sin(2\pi z/p),0)$ is mapped onto the equator. When one moves from $z = -p/2$ to $z = p/2$ in column 1, the director field starts from the orientation
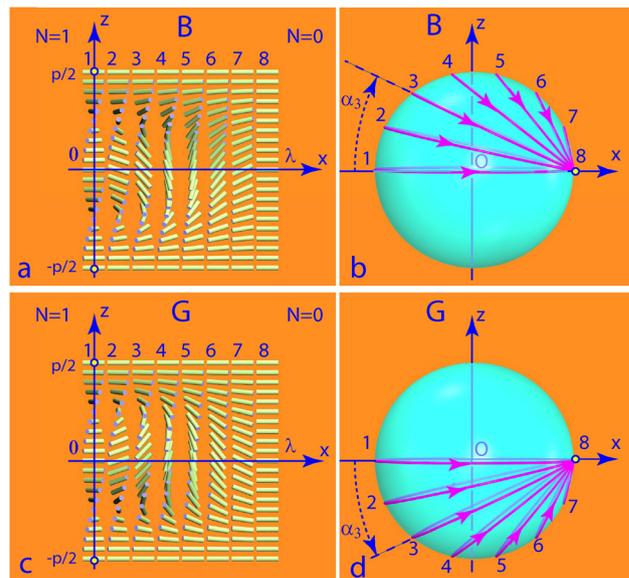

Fig. 8 Two variants, B and G, of a singularity-free director field of the dislocations with the Burgers vector $b = p$. (a) and (c) Director field. (b) and (d) Mapping of the director field on the unit sphere. The two variants are related by a rotation of π around the x axis.

$\mathbf{n}_B(0,-p/2) = (1,0,0)$, represented by the yellow dot (imposed by the anchoring on the lower mica sheet), and rotates by the azimuthal angle 2π around the z-axis until it returns to the the orientation $\mathbf{n}_B(0,p/2) = (1,0,0)$ imposed by the anchoring on the upper mica sheet. By this means, column 1 is mapped onto the equator.

Column 8 with $\mathbf{n}_B(\lambda,z) = (1,0,0)$ is mapped as a whole onto the yellow dot.

The intermediate columns labeled as $i = 2,...,7$ are mapped successively on circles making angles $\alpha_i = (i-1)\pi/14$ with the equator and passing through the yellow dot $(1,0,0)$.

The analytical expression of the director field of the B variant is given in Section 1.1 of the SI.

3.2 G variant of the singularity-free director field of dislocations with the Burgers vector $b = p$

The director field $\mathbf{n}_G(x,z)$ of the second, G variant of the singularity-free director field of dislocations with the Burgers vector $b = p$ is represented graphically in Fig. 8c. It is related to the variant B by rotation of the field $\mathbf{n}_B(x,z)$ as a whole by π around the x-axis.

When mapped on the unit sphere, the field $n_G(x,z)$ covers the whole south hemisphere. Its columns, labeled $i = 1,...,8$, are mapped on circles making angles $\alpha_i = -(i-1)\pi/14$ with the x axis.

3.3 GG and BB dislocation pairs are immune against annihilation

Dislocations of the G- and B-types can form four types of pairs: GG, BB, GB and BG.

The director field of the GG pair is depicted in Fig. 9. Here, the dislocation on the right labeled as G′ is of the G-type.
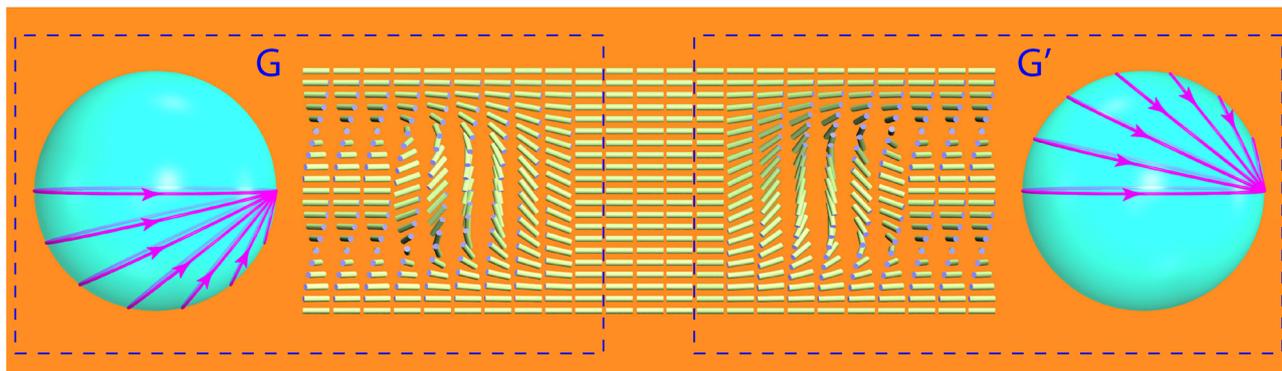
Fig. 9 Construction of the Lehmann cluster from two G-type singularity-free dislocations defined in Fig. 8. The director field of the dislocation G' is obtained from dislocation G by rotation as a whole by π around the z-axis. Director fields of the two dislocations are matched by a band of a uniform field $\mathbf{n}$ = (1,0,0).

It is related to the dislocation G on the left by rotation of π around the z axis. The space between the G and G' dislocations is filled by the uniform field (1,0,0).

Fig. 10 shows that the mapping of the director field of the GG' pair covers completely the unit sphere independently of the distance δ between dislocations. For this topological reason, the GG' pair is immune against annihilation.

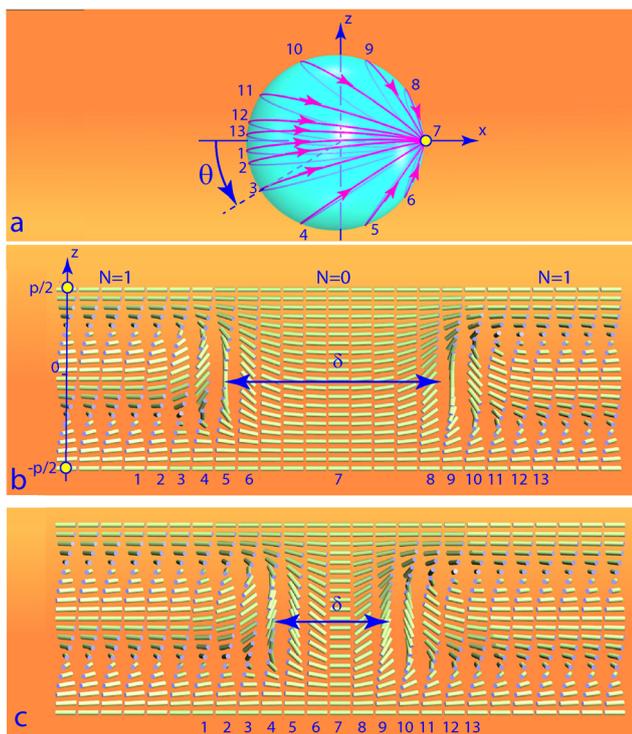The same conclusion is reached in the case of the BB pair.

Fig. 10 Immunity against annihilation of the GG' dislocation pair defined in Fig. 9. (a) Mapping on the unit sphere of director fields shown in (b) and (c). No matter what is the distance δ between the dislocations, the whole unit sphere is covered completely because the angle θ varies always from 0 to 2π. For this reason, the GG' pair of dislocations is immune against annihilation.

3.4 GB and BG pairs are subjected to annihilation

The director field of the GB pair is depicted in Fig. 11. Here, the dislocation on the right labeled as B' is of the B-type. It is related to the dislocation B defined in Fig. 8b by rotation of π around the z axis. The space between the G and B' dislocations is filled by the uniform field (1,0,0).

Fig. 12 shows that the mapping of the director field of the GB' pair covers only partially the south hemisphere. The area Σ covered by the mapping decreases with the distance δ between dislocations. In the limit $\Sigma \to 0$, the annihilation occurs. The same conclusion is reached in the case of the BG pair.

We can conclude that stable GB and BG pairs of dislocations should not exist, which actually is confirmed by our experiments.

4 Structure and energy of Lehmann clusters

4.1 Orientation of Lehmann clusters

In the previous section, we have assumed arbitrarily that dislocations forming Lehmann clusters inside the $N = 1$ annular field are orthogonal to the anchoring direction. Now, experiments reported in Section 2.3 (see Fig. 5b–d) show that the Lehmann clusters can have arbitrary orientations. It is therefore necessary to ask how the director field of a Lehmann cluster depends on its orientation defined in Fig. 13a, *i.e.*, on the angle γ that it makes with the direction of the anchoring which is assumed to be the same on both mica sheets.

4.2 Dependence of the structure on the orientation angle γ

For the sake of simplicity, let us consider again the case of Lehmann clusters inside the $N = 1$ field.

The case of the Lehmann cluster orthogonal to the anchoring direction corresponds to $\gamma = \pi/2$ (see Fig. 13a) and its director field, represented in the first column and the second row of Fig. 13c, is the same as the one in Fig. 10c.

Starting from this director field $\mathbf{n}_{\pi/2}(\xi,z)$, it is easy to obtain fields $\mathbf{n}_\gamma(\xi,z)$, corresponding to other values of the angle γ, by a simple geometrical transformation: a rotation of the director by
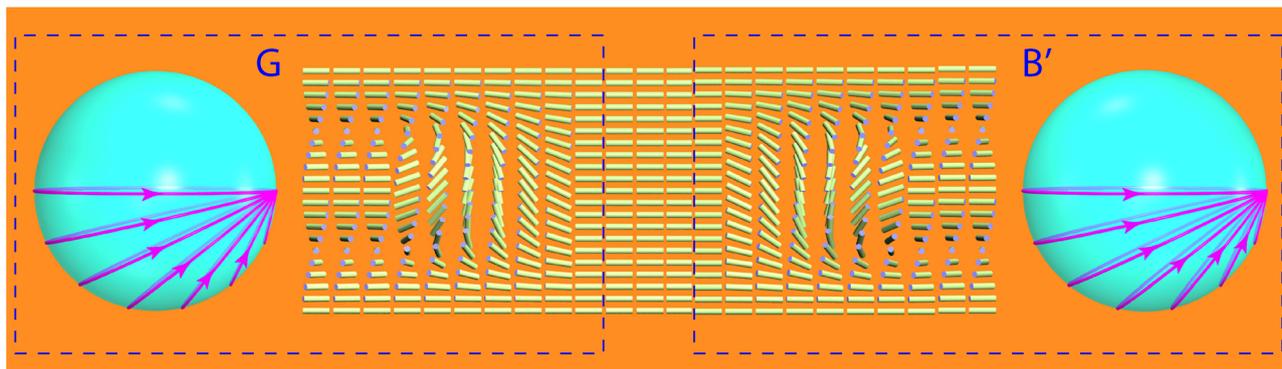
Fig. 11 Pair of the G-type and B-type singularity-free dislocations defined in Fig. 8. The director field of the dislocation B' is rotated as a whole around the z-axis by π with respect to the dislocation B. Director fields of the two dislocations are matched by a band of a uniform field **n** = (1,0,0).
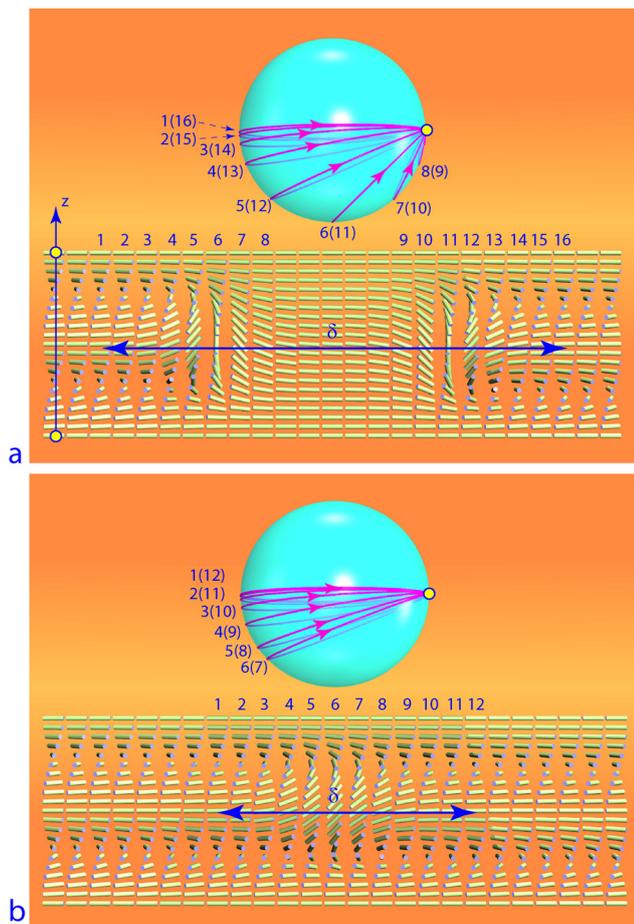

Fig. 12 Singularity-free director field of the dislocation pair GB′ defined in Fig. 11 is subjected to annihilation. (a) Mapping of the director field on the unit sphere for a large distance δ between dislocations. Only the south hemisphere is covered by the mapping. (b) When the distance δ decreases, the surface Σ covered by the mapping shrinks. In the limit $\Sigma \to 0$, the annihilation occurs. For this reason, stable pairs of the GB′ type have not been observed in experiments.

the angle $\psi = \gamma - \pi/2$ around local vertical axes ζ_ξ (parallel to z) passing through the point ξ on the horizontal axis ξ. For $\psi < 0$

and $\psi > 0$, rotations are respectively in anticlockwise and clockwise directions.

In Fig. 13c, we represent the set of eight fields, obtained by this method, corresponding to $\gamma = 0, \pi/4, 2\pi/4,\ldots,7\pi/4$.

4.3 Energy *versus* the orientation angle γ: theory

All eight configurations of the director field $\mathbf{n}_\gamma(\xi,z)$ have right-hand twist distortions in the z direction.

There is also a twist distortion in the horizontal ξ direction, but its sign and amplitude depend on the angle γ. As shown in Fig. 13c, in the field $\mathbf{n}_0(\xi,z)$, the twist is right-handed, *i.e.* the same as in the z direction, while in the field $\mathbf{n}_\pi(\xi,z)$, the twist distortion has opposite handedness. For this reason, the energy per unit length of Lehmann clusters $E_{\rm LC}(\gamma)$ in the configuration labeled $\gamma = 0$ shown in Fig. 13c (first column, first row) is expected to be lower than that of the configuration $\gamma = \pi$ (first column, third row).

Numerical calculation of the energy $E_{\rm LC}(\gamma)$ of the configurations shown in Fig. 13c (see SI Section 1.2) confirms this expectation: the blue line plot of $E_{\rm LC}(\gamma)$ in Fig. 13b has a minimum for $\gamma = 0$ and a maximum for $\gamma = \pi$.

It is stressed that in the diagram of Fig. 13b, there is a second plot drawn with a red line which is obtained by shifting the blue line by π. Its presence is required by symmetry: as the anchoring direction is represented in Fig. 13a by a two headed arrow, the angle γ is equivalent to $\gamma + \pi$. Therefore, for each value of γ, two configurations of the director field with different energies $E_{\rm LC}(\gamma)$ and $E_{\rm LC}(\gamma + \pi)$ are possible. In Fig. 13b, plots with thick red and blue lines correspond to configurations with lower energies.

4.4 Energy *versus* the orientation angle γ: experiments

The dependence of the energy of Lehmann clusters T on their orientation γ with respect to the anchoring has been detected in experiments performed with a cylinder/cylinder wedge of minimal thickness $h_{\rm min} < p/2$. In Fig. 14, we show changes in the direction of Lehmann clusters driven by the torque $\Gamma = \partial T/\partial \gamma$.

Let us consider, for example, the behavior of the Lehmann cluster LC1 in Fig. 14a–c. Shortly after its generation by the cholesteric $\to$ isotropic $\to$ cholesteric phase sequence, the Lehmann cluster LC1 is not orthogonal to the adjacent $p/2$
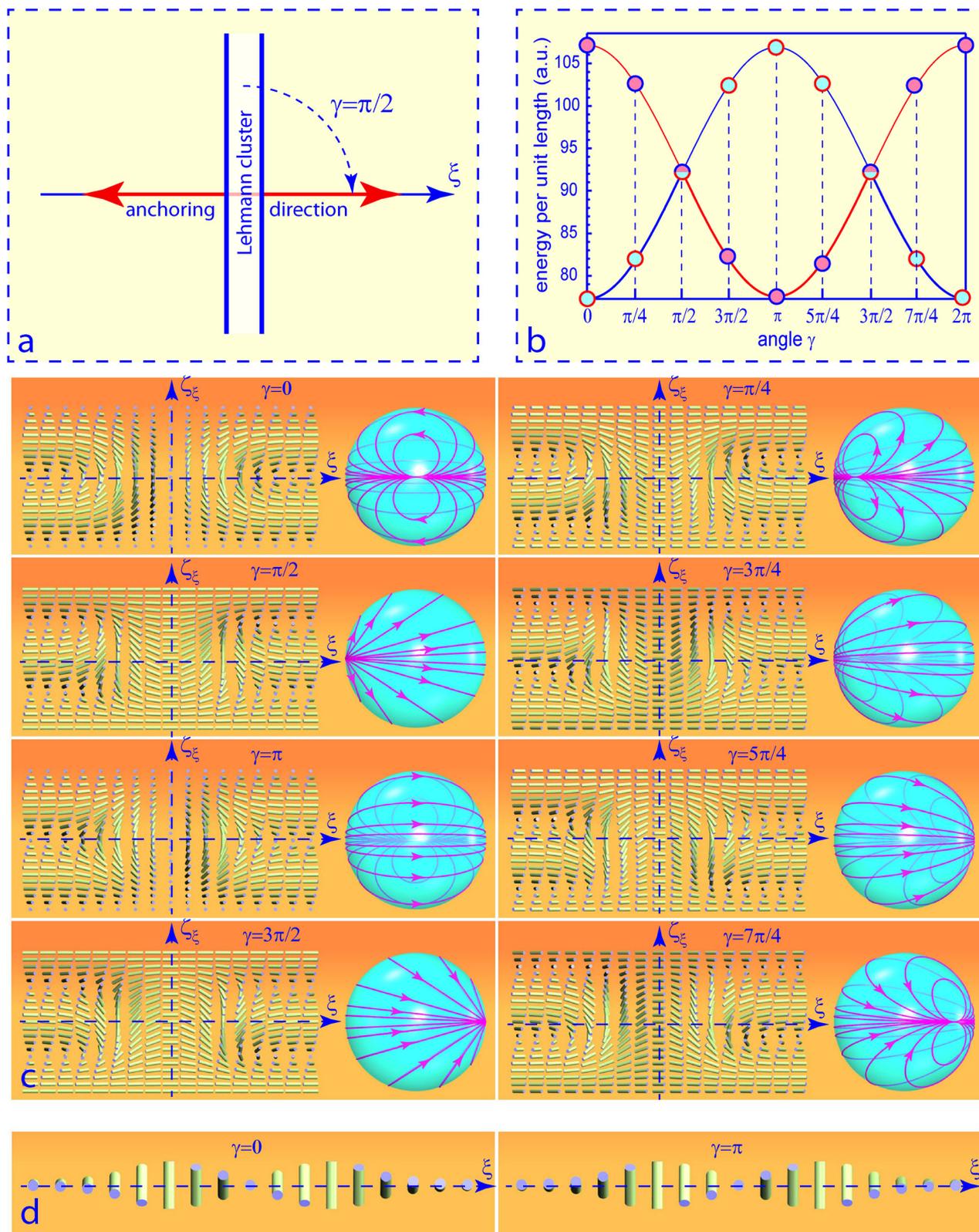
Fig. 13 Dependence of the structure and energy of Lehmann clusters on their orientation with respect to the anchoring. (a) Definition of the angle γ between a Lehmann cluster and the anchoring direction. (b) Variation of the energy with the orientation angle γ. (c) Dependence of the director field of Lehmann clusters on their orientation angle γ. (d) Twist distortions along the horizontal axis ξ for $\gamma = 0$ and $\gamma = \pi$.
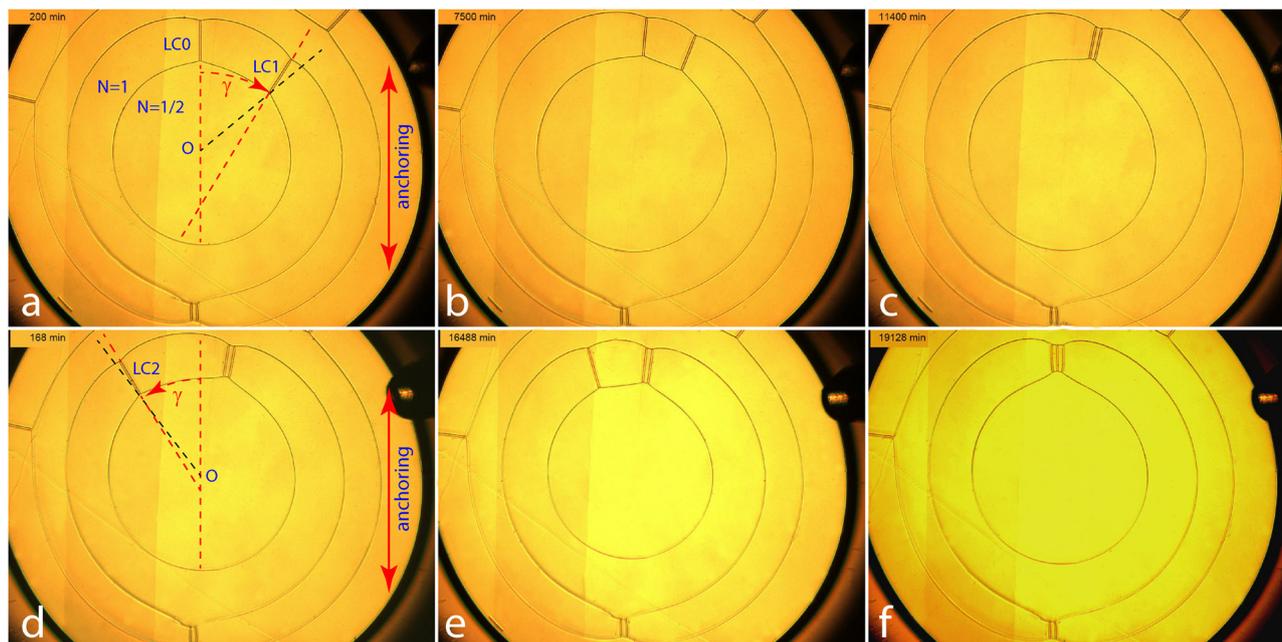
Fig. 14 Evolution of the orientation of Lehman clusters. The orientation of the Lehman cluster LC0 parallel to the anchoring corresponds to the minimum of its energy. (a) Shortly after its generation, the new Lehmann cluster LC1 is not orthogonal to the adjacent $p/2$ concentric dislocation loops because there is an elastic torque acting on it due to the torque $\Gamma = \partial T/\partial \gamma$. (b) and (c) The subsequent orthoradial drift of the Lehmann cluster LC1 toward LCO reduces its length and tension $T(\gamma)$. (d)–(f) The same behavior is observed with the Lehmann cluster LC2. Note that the final collision between Lehmann clusters does not result in annihilation (see Videos S2 and S3 of the SI).

concentric dislocation loops because the elastic torque $\Gamma = \partial T/\partial \gamma$ acts on. On a longer time scale, the Lehmann cluster slowly drifts toward the orientation parallel to the anchoring direction corresponding to the minimum of the tension $T(\gamma)$.

The Lehmann cluster LC2 generated subsequently has the same behavior: it also drifts toward the orientation of the anchoring (see Fig. 14d–f) (see Video 2 of the SI).

Through these two generation-drift processes, a stable set of three Lehmann clusters gathered together is shown in Fig. 14f. In Section 5, we will explain why, in this set, the Lehmann clusters are protected against annihilation.

4.5 Energy and structure *versus* the z position

Above, for the sake of simplicity, we considered Lehmann clusters embedded in the field $N = 1$. In practice, as shown in Fig. 15, Lehmann clusters can also be embedded in a thicker field, for example, $N = 5/2$. In this case, the structure and the energy per unit length T of a Lehmann cluster depend not only on its orientation but also on the level z inside the sample. When the orientation of the Lehmann cluster is given by the azimuthal angle γ and its position inside the stack by the coordinate z, then its energy T depends, in principle, on both variables: $T = T(\gamma, z)$. However, the energy T should be invariant with respect to the operations of the screw symmetry axis of the cholesteric helix. This requirement is satisfied when the tension T depends only on the linear combination $\psi = \gamma - 2\pi z/p$ where p is the local pitch of the cholesteric helix:

$$T = T(\gamma - 2\pi z/p) \qquad (7)$$

5 Larger sets of dislocation topologically protected against annihilation

5.1 Gathering together of Lehmann clusters

In the experiment depicted in Fig. 5, new Lehmann clusters have been generated inside the $N = 1$ field by local cholesteric → isotropic → cholesteric phase transitions. Experiments show that Lehmann clusters generated by this method inside the same annular field labeled N between two adjacent $b = p/2$ dislocations have tendency to gather together due to an attractive interaction involving their own tension as well as the tensions of the $b = p/2$ dislocations.

For example, in Fig. 5b–d, two Lehmann clusters are gathered together inside the $N = 3/2$ annular field, while in Fig. 16a, three Lehmann clusters are gathered together inside the $N = 1$ field.

5.2 Immunity against annihilation of colliding Lehmann clusters

We will point out now that the stability of sets of several Lehmann clusters gathered together is of the same topological nature as the stability of the individual Lehmann clusters made of two dislocations with opposite Burgers vectors $b = p$ and $b = -p$.

5.3 Models of the director field of the set of three Lehmann clusters

For this purpose, let us consider models of the director field inside cross sections (ξ, z) defined in Fig. 16a. In Fig. 16c, we
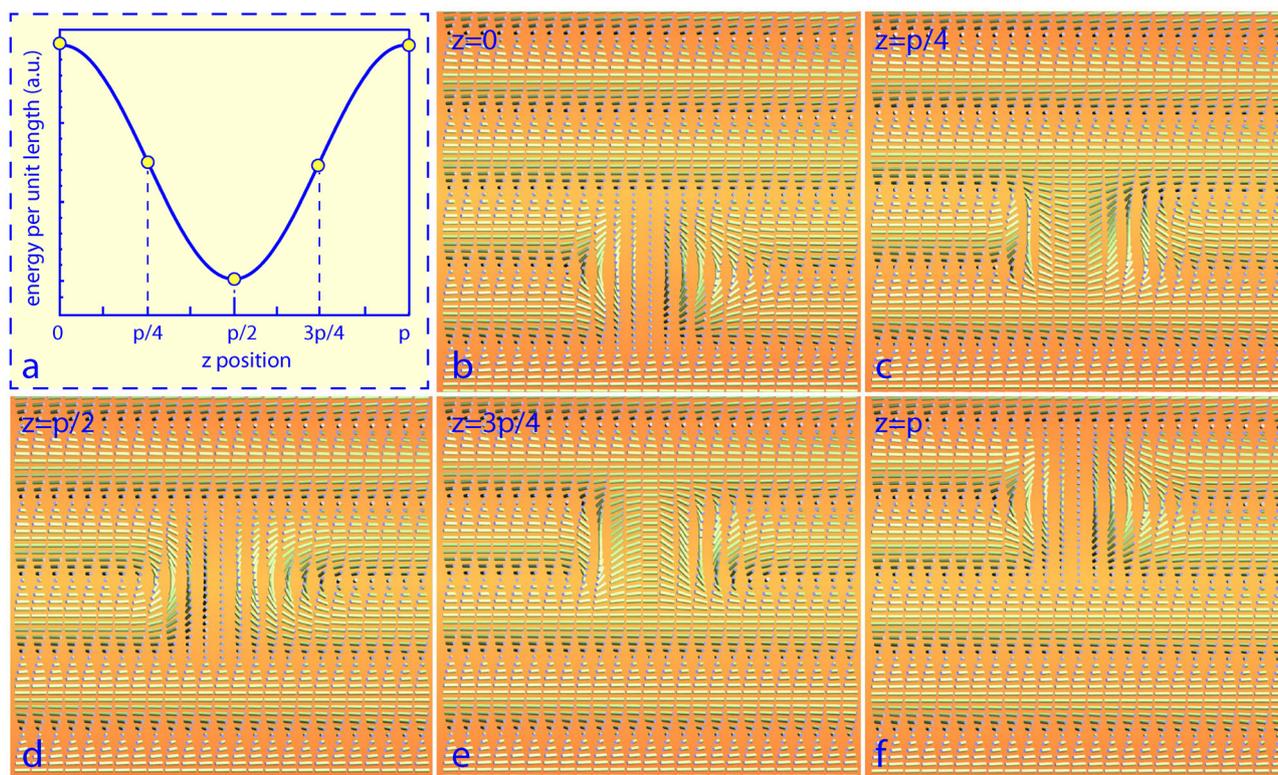
Fig. 15 Dependence of the structure and energy of Lehmann clusters on their z position inside a sample of thickness "$N = 2.5$". (a) Dependence of the energy of Lehmann clusters on their z position. (b)–(f) Dependence of the structure of Lehmann clusters on their z position.

show four models corresponding to different orientations of the three Lehmann clusters with respect to the anchoring direction defined in Fig. 16b.

When the Lehmann clusters are orthogonal to the anchoring direction, their director field has structures depicted in the first and third rows of Fig. 16c labeled as GG′ or BB′ previously. In these two cases, the director at the mid-height of the sample ($z = 0$) stays in the plane (ξ_1,z) or (ξ_3,z) and rotates by the angle θ in the anticlockwise or clockwise direction as already discussed above.

On the other hand, when Lehmann clusters are parallel to the anchoring direction, their director field has structures depicted in the second and fourth rows of Fig. 16e. Here, the director at the mid-height of the sample ($z = 0$) is orthogonal respectively to the ξ_2 and ξ_4 axes and rotates by the angle θ around them in anticlockwise or clockwise directions.

A model of the director field of this set of three Lehmann clusters in the (ξ_1,z) cross section defined in Fig. 16a is shown in Fig. 16d. When mapped on the unit sphere in Fig. 16e, it covers it three times. For $z = 0$, the director rotates by $\theta(\xi_1)$ in the (ξ_1,z) plane and can be expressed as

$$\mathbf{n}(x,0,0) = [\cos\theta(x),0,\sin\theta(x)] \qquad (8)$$

where the function $\theta(\xi_1)$ is monotonically growing from 0 to 6π. Fig. 16f shows that the director fields $\mathbf{n}(\xi_2,0)$ and $\mathbf{n}(\xi_4,0)$ form respectively right-hand and left-hand helices. As in the mixtures of 5CB with CB15, the cholesteric helix is dextrogyre; therefore,

the structure of the Lehmann clusters depicted in the second row of Fig. 16e has the lowest energy.

6 Skyrmionic topology perspective

It is instructive to analyze the structures discussed above from the perspective of topological solitons like skyrmion and fractional skyrmion tubes.[10,11] This analysis can also help connecting the fundamental aspects of our findings in liquid crystals with those in other physical systems, like colloidal and solid-state magnets and optics.[10–18]

6.1 Vectorization of the nonpolar director's order parameter

The director fields of nonsingular solitonic structures corresponding to $b = p$ quasi-layer dislocations that we study here can be smoothly vectorized by decorating the rod-like molecules with unit vectors of different orientations in three dimensions.[19] Such vectorization converts the nonpolar director's order parameter space of S^2/Z_2 into S^2. This is possible because all two-dimensional (and ones with higher dimensionality) topological soliton objects can be smoothly vectorized without creating any extra singularities.[10] The process of decorating the nematic director field lines with vectors has the actual physical implementation in molecular-colloidal chiral liquid crystal systems where magnetically monodomain colloidal particles can be doped into the nonpolar molecular nematic host medium, so that unit vectors due to magnetic moments of
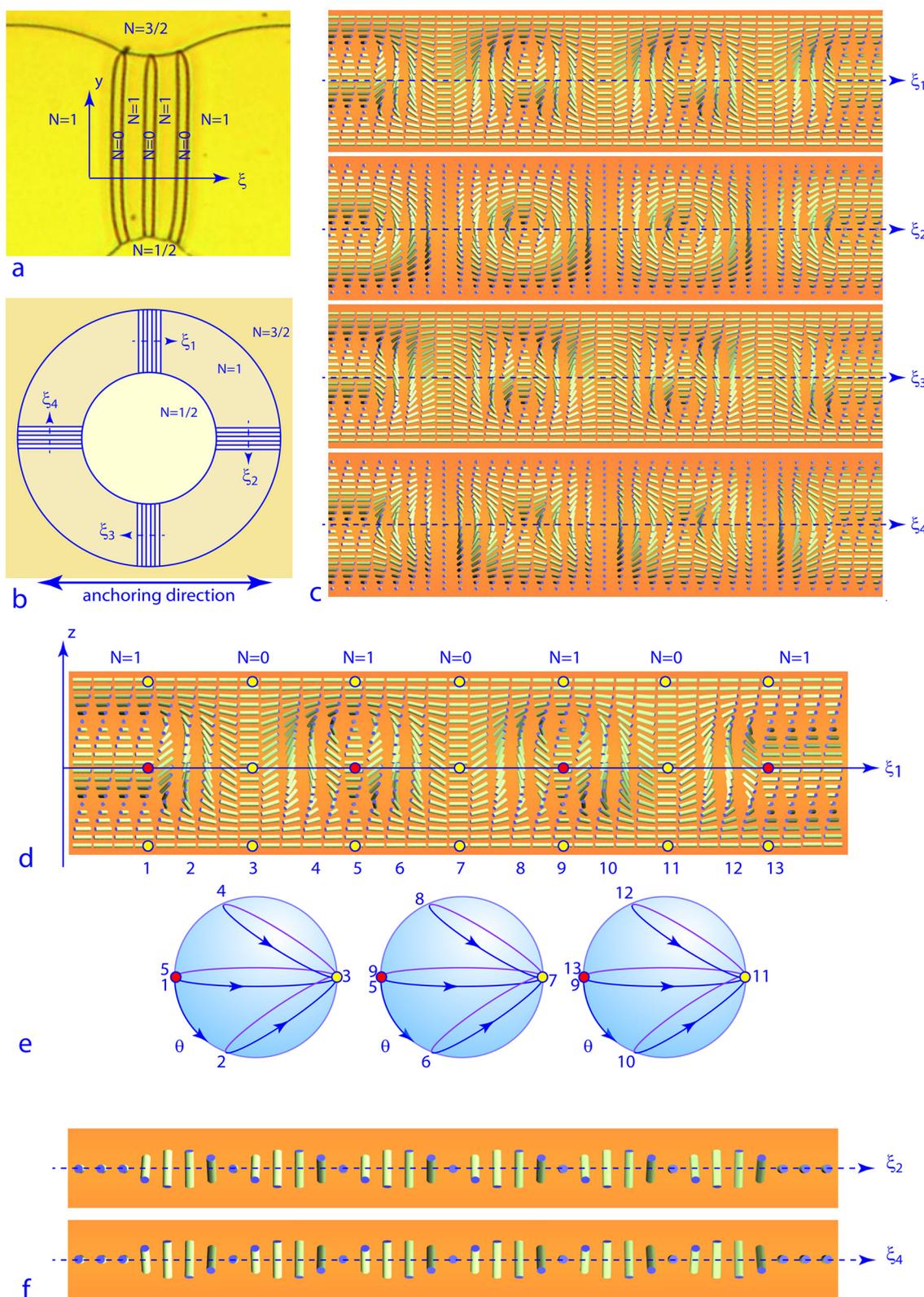
Fig. 16 Topologically protected sets of three Lehmann clusters. (a) View in a microscope. (b) Four different orientations of Lehmann clusters with respect to the anchoring direction. (c) Director fields corresponding to the four orientations defined in (b). (d) Singularity-free model of the director field in the (ξ_1, z) cross section along the ξ_1-axis, defined in (a), which is parallel to the anchoring direction on mica surfaces. (e) The mapping of the director field onto the unit sphere covers it three times. (f) The director field at mid-height $z = 0$ along the ξ_2-axis forms a right-hand helix, while along the ξ_4-axis, the helix is levogyre.

the nanoplates align in one of the two non-distinguishable orientations of the director with nonpolar symmetry.[13] The finite-length fragments of Lehman clusters (skyrmion tubes) in a bulk of chiral nematic are known terminating on point defects,[11] which, similar to skyrmion tubes themeselves, can be also smoothly vectorized.

6.2 Equivalence between the Lehmann clusters and skyrmion tubes

From the homotopy theory, $\pi_2(S^2) = Z$.[10,20] Therefore, topologically stable skyrmion tubes are allowed and expected in chiral nematics, similar to a host of other media in which such configurations have been studied recently.[11,17] In fact, Lehman clusters have been previously identified as such objects in both nonpolar molecular and ferromagnetic colloidal chiral liquid crystals.[13,20]

Since the homotopy theory description of skyrmion tubes and singular point defects in 3D is similar, with $\pi_2(S^2) = Z$,[10,19,21,22] it is natural that the fragments of the skyrmion tubes would terminate at the the topological objects with monopole topology of the same homotopy class $\pi_2(S^2) = Z$,[11] which can be found in the micrographs shown in Fig. 4d and in Fig. 17.

6.3 Equivalence between $b = p$ dislocations and merons

Each interacting nonsigular quasi-layer dislocation can be interpreted as a meron (also often referred to as "half-skyrmion").[11,15,16] Depending on the relative signs of the fractional skyrmions numbers of merons, they can either annihilate (for the case of opposite signs) or combine into a composite topological soliton with an integer-valued skyrmion number.[18] We note that the relative signs of the skyrmion numbers can be determined upon smooth vectorization of the director field, though the

procedure of mapping the director field patterns onto the two-sphere that we use is equivalent to it because S^2 is the order parameter space for the unit vector field in 3D.

6.4 Skyrmions and merons embedded into helical background

The skyrmions and merons embedded into helical background have been explored extensively in chiral non-centrosymmetric magnets and light fields,[15,16,23] in magnetic colloidal liquid crystals,[13] as well as other research fields where they often have structures vividly similar to the quasi-layer dislocations and Lehman clusters in chiral nematic liquid crystals.[6,10,15,16,24] From the skyrmionic topology perspective, the three Lehman clusters shown in Fig. 3a are skyrmion tubes of the same elementary skyrmion number, each composed of pairs of merons in the form of inter-bonded quasi-layer dislocations of B–B or G–G type in the helicoidal director field, interacting with each other repulsively. In addition to the prevalent case of the two merons (dislocations) being located at the same depth level, situations can arise when the dislocations would be localized at different levels of the quasi-layered system of the chiral nematic medium (see such an example in Fig. 15a and b in ref. 1). In this case, additional energetic stability can be endowed to the dislocations (merons) by the need of continuity of helical quasi-layers that separate them.

6.5 Chiral nematics as a playground of merons and skyrmions: fundamentals and utility

The high experimental accessibility of chiral nematic liquid crystals allows us to see in great detail the processes of annihilation and hybridization of merons that in the end form topologically stable skyrmion tubes. While the structures we depict are shown in highly simplified schematic forms, which
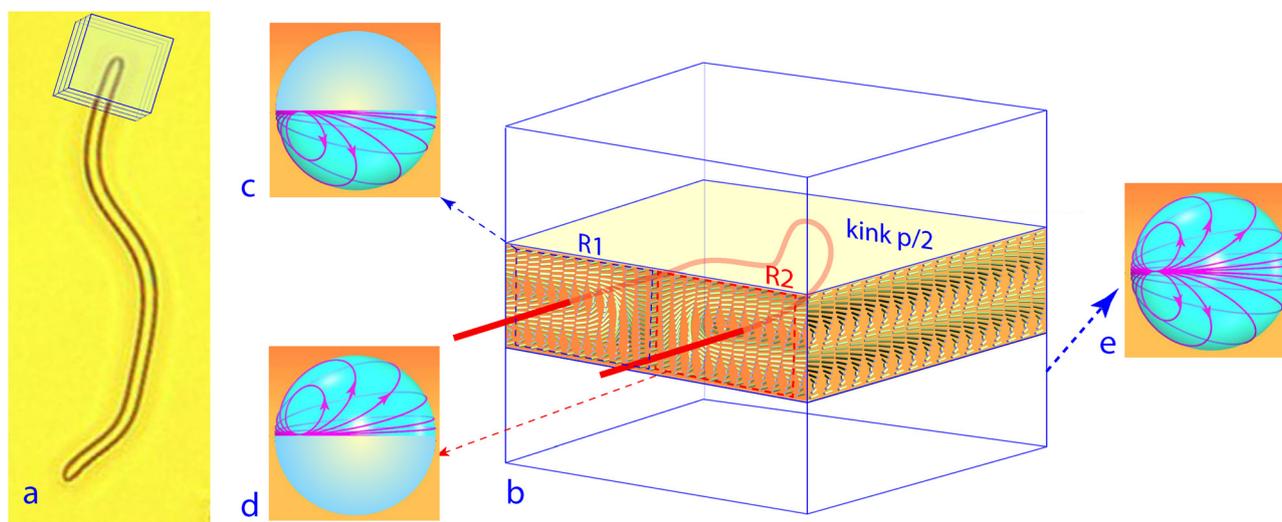

Fig. 17 Monopoles located at extremities of a skyrmion tube of finite length. (a) Lehmann cluster of finite length observed in experiments (see Fig. 4d). It is equivalent to a skyrmion tube. One of its extremities is located inside a cuboid box. (b) Director field on surfaces of the cuboid. (c) Director field from the rectangle R1 covers the south hemisphere. (d) Director field from the rectangle R2 covers the north hemisphere. (d) Director field from the surface of the whole cuboid covers the whole unit sphere. Note the presence of a $p/2$ kink on the U-turn of the dislocation forming the skyrmion tube (Lehmann cluster).

allow us to directly convey the implications of mappings from physical configurational space to order parameter space in terms of topological protection and stability, we note that geometrically different but topologically the same configurations can be observed when the axes of the skyrmion or meron tubes are smoothly translated across the depth of the sample (helical axis).

The topological and energetic stability of such structures may allow for their technological utility in applications like guiding beams of light.[25–27] In the past, structures of optical axis associated with various defects and topological solitons were utilized in controlling light mainly in non-chiral nematic media, whereas the opportunities that can be potentially presented by the chiral nematic topological solitons have been largely overlooked despite the fact that they would be capable of guiding and steering laser light,[26,27] calling for future research in this direction.

7 Conclusions and outlook

The very good experimental accessibility of liquid crystalline topological structures allowed us to explore the nature of nonsingular quasi-layer dislocations and their interactions when embedded within the chiral nematic's helical background, demonstrating how Lehman clusters and $b = p$ dislocations can be understood as translationally invariant skyrmion and meron tubes. We demonstrated that the stability of these objects is enhanced by the phenomenon known in the liquid crystal field as the "escape into the third dimension" of the director field, effectively endowing the chiral topological soliton nature to these structures. We showed that from a topological point of view, the Lehmann clusters can be interpretted as skyrmion tubes, with topologically monopole-like structures at their extremities in the case of their finite length. Our findings may provide vivid insights into solitonic-topology-enriched physical behavior that could have analogues in other research fields, like magnetism and optics and pure mathematics,[12,15,17,27–33] as well as could have technological utility ranging from waveguiding laser light[26–28] to the control of surface topography in cholesteric elastomers. The study of similar objects in magnets has the potential for enabling various new types of data storage,[15] where our work presented here could serve as an inspiration.

Conflicts of interest

There are no conflicts to declare.

Data availability

The data supporting this article have been included as part of the supplementary information (SI). Supplementary information: the list of the videos quoted in the article. See DOI: https://doi.org/10.1039/d5sm01244a.

Acknowledgements

Notes and references

1 I. Smalyukh and O. Lavrentovich, *Phys. Rev. E: Stat., Nonlinear, Soft Matter Phys.*, 2002, **66**, 051703.

2 M. Kleman and J. Friedel, *J. Phys. Colloq.*, 1969, **30**, C4–43.

3 B. A. Wood and E. L. Thomas, *Nature*, 1986, **324**, 655–657.

4 S. D. Hudson and E. L. Thomas, *Phys. Rev. A: At., Mol., Opt. Phys.*, 1991, **44**, 8128.

5 P. Pieranski, M. Zeghal, M. H. Godinho, P. Judeinstein, R. Bouffet-Klein, B. Liagre and N. Rouger, *Phys. Rev. Lett.*, 2023, **131**, 128101.

6 P. Pieranski and M. Godinho, *Liq. Cryst.*, 2024, **51**, 2144–2175.

7 P. Pieranski and M. H. Godinho, *C. R. Phys.*, 2024, **25**, 367–388.

8 J.-Y. Lee, M. Zeghal, P. Judeinstein, M. H. Godinho, I. Smalyukh and P. Pieranski, *Soft Matter*, 2025, **21**, 8205–8218.

9 P. Pieranski, *Liq. Cryst. Rev.*, 2022, **10**, 3–33.

10 I. I. Smalyukh, *Rep. Prog. Phys.*, 2020, **83**, 106601.

11 J.-S. Wu and I. I. Smalyukh, *Liq. Cryst. Rev.*, 2022, **10**, 34–68.

12 N. Nagaosa and Y. Tokura, *Nat. Nanotechnol.*, 2013, **8**, 899–911.

13 Q. Zhang, P. J. Ackerman, Q. Liu and I. I. Smalyukh, *Phys. Rev. Lett.*, 2015, **115**, 097802.

14 R. D. Kamien and R. A. Mosna, *New J. Phys.*, 2016, **18**, 053012.

15 A. Fert, N. Reyren and V. Cros, *Nat. Rev. Mater.*, 2017, **2**, 1–15.

16 H. Kedia, I. Bialynicki-Birula, D. Peralta-Salas and W. T. Irvine, *Phys. Rev. Lett.*, 2013, **111**, 150404.

17 B. Wang, Z. Che, C. Cheng, C. Tong, L. Shi, Y. Shen, K. Y. Bliokh and J. Zi, *Nature*, 2025, **638**, 394–400.

18 J.-S. B. Tai, A. J. Hess, J.-S. Wu and I. I. Smalyukh, *Sci. Adv.*, 2025, **10**, eadj9373.

19 P. J. Ackerman, R. P. Trivedi, B. Senyuk, J. van de Lagemaat and I. I. Smalyukh, *Phys. Rev. E: Stat., Nonlinear, Soft Matter Phys.*, 2014, **90**, 012505.

20 R. Voinescu, J.-S. B. Tai and I. I. Smalyukh, *Phys. Rev. Lett.*, 2020, **125**, 057201.

21 G. Toulouse and M. Kleman, *J. Phys. Lett.*, 1976, **37**, 149.

22 G. Toulouse, *"Sens d'une exploration" dans Le goût de la science*, Alvik, Paris, 1st edn, 2005.

23 M. Berry and M. Dennis, *Proc. R. Soc. A*, 2001, **111**, 2251–2263.

24 J.-S. B. Tai, P. J. Ackerman and I. I. Smalyukh, *Proc. Natl. Acad. Sci. U. S. A.*, 2018, **115**, 921–926.

25 C. Meng, J.-S. Wu and I. I. Smalyukh, *Nat. Mater.*, 2023, **22**, 64–72.

26 G. Poy and S. Žumer, *Opt. Express*, 2020, **28**, 24327.

27 G. Poy, A. J. Hess, I. I. Smalyukh and S. Žumer, *Phys. Rev. Lett.*, 2020, **125**, 077801.

28 A. J. Hess, G. Poy, J.-S. B. Tai and S. Z. Žumer, *Phys. Rev. X*, 2020, **10**, 031042.

29 U. Tkalec, M. Ravnik, S. Čopar, S. Žumer and I. Muševič, *Science*, 2011, **333**, 62–65.

30 L. H. Kauffman and S. Lambropoulou, *Adv. Appl. Math.*, 2004, **33**, 199–237.

31 P. Pieranski and M. H. Godinho, *Eur. Phys. J.: Spec. Top.*, 2024, 1–21.

32 B. Zappone and R. Bartolino, *Proc. Natl. Acad. Sci. U. S. A.*, 2021, **118**, e2110503118.

33 L. H. Kauffman and S. Lambropoulou, *Topology in Molecular Biology*, Springer, 2007, pp. 69–110.